Thermodynamics of the Interaction between *O*-Acetylserine Sulfhydrylase and the C-Terminus of Serine Acetyltransferase†

Sangaralingam Kumaran and Joseph M. Jez*

Donald Danforth Plant Science Center, 975 North Warson Road, St. Louis, Missouri 63132

Received January 19, 2007; Revised Manuscript Received March 9, 2007

ABSTRACT: Cysteine biosynthesis in plants is partly regulated by the physical association of *O*-acetylserine sulfhydrylase (OASS) and serine acetyltransferase (SAT). Interaction of OASS and SAT requires only the 10 C-terminal residues of SAT. Here we analyze the thermodynamics of formation of a complex of *Arabidopsis thaliana* OASS (AtOASS) and the C-terminal ligand of AtSAT (C10 peptide) as a function of temperature and salt concentration using fluorescence spectroscopy and isothermal titration calorimetry (ITC). Our results suggest that the C-terminus of AtSAT provides the major contribution to the total binding energy in the plant cysteine synthase complex. The C10 peptide binds to the AtOASS homodimer in a 2:1 complex. Interaction between AtOASS and the C10 peptide is tight (K_d = 5−100 nM) over a range of temperatures (10−35 °C) and NaCl concentrations (0.02−1.3 M). AtOASS binding of the C10 peptide displays negative cooperativity at higher temperatures. ITC studies reveal compensating changes in the enthalpy and entropy of binding that also depend on temperature. The enthalpy of interaction has a significant temperature dependence (ΔC_p = −401 cal mol^{-1} K^{-1}). The heat capacity change and salt dependence studies suggest that hydrophobic interactions drive formation of the AtOASS·C10 peptide complex. The potential regulatory effect of temperature on the plant cysteine synthase complex is discussed.

Cysteine synthesis in plants and bacteria occurs through a two-step pathway that connects the nitrogen and sulfur assimilation processes (*1*−*3*). In the first step of the cysteine biosynthetic pathway (Figure 1), serine acetyltransferase (SAT,[1] EC 2.3.1.30) generates the activated sulfide acceptor *O*-acetylserine from serine and acetyl-CoA. *O*-Acetylserine sulfhydrylase (OASS, EC 4.2.99.8) catalyzes the final step by inserting sulfide into *O*-acetylserine in a β-replacement reaction to yield cysteine and acetate. In addition to feedback inhibition by cysteine, biochemical regulation of this pathway involves the physical association of SAT and OASS which form the cysteine synthase complex. This macromolecular assembly is not involved in metabolite channeling because *O*-acetylserine freely diffuses out of the complex (*4*−*6*). Instead, interaction of the two proteins appears to coordinate sulfate assimilation and modulates cysteine synthesis at the cellular level in plants (*7*). The physiological role of the complex in bacteria is not as well defined, but the complex may serve a similar function.

Protein−protein interactions between SAT and OASS modulate the activity of each enzyme. In the plant cysteine synthase complex, SAT activity increases and OASS activity decreases (*6*, *8*). This results in production of *O*-acetylserine, which is used by free OASS to generate cysteine (Figure 1). Under low-sulfur conditions, *O*-acetylserine accumulates, which disrupts formation of the cysteine synthase complex and results in downregulation of SAT activity. Increased *O*-acetylserine concentrations activate expression of genes required for sulfate uptake and sulfur assimilation pathways. As sulfur concentrations increase, *O*-acetylserine levels decrease and the cysteine synthase complex reassociates. Demonstration of complex formation using the proteins from plants and bacteria has employed size-exclusion chromatography, yeast two-hybrid analysis, surface plasmon resonance, and fluorescence spectroscopy (*9*−*16*). These studies establish that only the 10−20-amino acid C-terminal tail of SAT is essential for association with OASS (*9*−*12*, *16*). Crystal structures of *Arabidopsis thaliana* OASS (AtOASS) and *Haemophilus influenzae* OASS in complex with peptides corresponding to the C-termini of their cognate SAT (C10 peptide) reveal that the OASS active site forms the binding site for the C-terminus of SAT (*17*, *18*). Because binding of the C10 peptide blocks access to the catalytic center of OASS, this explains how OASS activity is downregulated upon formation of the cysteine synthase complex. Moreover, comparison of the plant and bacterial structures suggests that structural plasticity in the active site allows for the binding of SAT C-termini with dissimilar sequences at structurally similar OASS active sites (*18*).

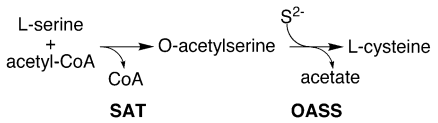

FIGURE 1: Overview of the reactions catalyzed by SAT and OASS.

†This work was supported by a grant from U.S. Department of Agriculture (NRI-2005−02518) to J.M.J.

* To whom correspondence should be addressed: Donald Danforth Plant Science Center, 975 N. Warson Rd., St. Louis, MO 63132. Telephone: (314) 587-1450. Fax: (314) 587-1550. E-mail: jjez@danforthcenter.org.

[1] Abbreviations: AtOASS, *Arabidopsis thaliana O*-acetylserine sulfhydrylase; AtSAT, *A. thaliana* serine acetyltransferase; C10 peptide, peptide corresponding to the 10 C-terminal residues of SAT; ITC, isothermal titration calorimetry; OASS, *O*-acetylserine sulfhydrylase; PLP, pyridoxal 5′-phosphate; SAT, serine acetyltransferase.

10.1021/bi7001168 CCC: $37.00 © 2007 American Chemical Society
Published on Web 04/11/2007

Understanding of the thermodynamic basis for formation of the cysteine synthase complex is required for the dissection of the regulatory mechanism underlying cysteine biosynthesis in plants and bacteria. A complete perspective of how these two enzymes form a macromolecular assembly requires knowledge of the structure, kinetics, and thermodynamics of complex formation. In this study, we examine the interaction between AtOASS and the *A. thaliana* SAT (AtSAT) C10 peptide by equilibrium binding studies using fluorescence spectroscopy and isothermal titration calorimetry (ITC). The stoichiometry and thermodynamics of complex formation confirm that AtOASS binds the AtSAT C10 peptide at each of two binding sites and reveal that negative cooperativity occurs at high temperatures. Our results indicate that binding of the C-terminus of SAT by OASS contributes a large portion of the total binding energy during formation of the plant cysteine synthase complex. This work provides insight into the energetics of complex formation and the thermodynamic basis for interaction of OASS and SAT.

EXPERIMENTAL PROCEDURES

Reagents. All buffers were prepared from reagent grade chemicals using double-distilled water that was further deionized using a Milli-Q purification system (Millipore Corp.). Recombinant wild-type AtOASS was expressed and purified as previously described (*14*). This enzyme is the cytosolic OASS isoform encoded by the At4g14880 gene in *A. thaliana*. The peptide corresponding to the 10 C-terminal residues of AtSAT (C10 peptide, YLTEWSDYVI) was synthesized by Sigma-Genosys. The AtSAT C10 peptide used here is from the sequence of At1g55920, which encodes the plastid localized enzyme; however, the core motif of the *A. thaliana* SAT C-termini [X(I/L)(S/T)EWSDY(V/I)I] is highly conserved in the plastid (At1g55920), cytosolic (At5g56760), and mitochondrial (At3g13110) isoforms. Although two additional SAT-like isoforms (At2g17640 and At4g35640) lacking this motif have been described, their extremely low in vivo expression levels and 100−1000-fold higher K_m values for acetyl-CoA and serine suggest that these isoforms do not contribute to cysteine synthesis (*19*). Protein and peptide concentrations were determined using molar extinction coefficients for the AtOASS homodimer (ϵ_{280} = 44 762 M^{-1} cm^{-1}) and the C10 peptide (ϵ_{280} = 8480 M^{-1} cm^{-1}), as described by Gill et al. (*20*).

Fluorescence Measurements. Titrations of AtOASS with the C10 peptide were performed by monitoring the intrinsic pyridoxal 5′-phosphate (PLP) fluorescence of AtOASS using a Cary Eclipse fluorimeter (Varian, Inc.). The excitation wavelength was 412 nm, and the fluorescence intensity was monitored at 505 nm. A 0.5 mL solution of AtOASS in a 2.0 mL quartz cuvette was equilibrated for 30 min at 22 °C. Scans of AtOASS (1 μM) were performed in 50 mM Hepes (pH 7) with 20 mM NaCl by adding 2 μL aliquots of C10 peptide in the same buffer to the cuvette containing AtOASS. Both excitation and emission slit widths were set to 5 nm, and the level of photobleaching under these conditions was less than 2%. Initial readings of both the sample and reference cuvette (containing only buffer) were used to define the initial fluorescence of the sample. The sample cuvette containing AtOASS was then titrated with peptide and the mixed solution equilibrated for 3 min. Data points from three such measurements were used to obtain the average fluorescence intensity change. Background signal was subtracted from sample fluorescence to obtain the relative emission increase upon C10 peptide binding. All measurements were corrected for dilution and inner filter effects (*21*). The extinction coefficient of the PLP in AtOASS is independent of salt concentration.

For determination of the ionic dependence of peptide binding, experiments used the same protocol described above with varied NaCl concentrations (0.02−1.3 M). At lower salt concentrations (<0.5 M NaCl), C10 peptide binding was analyzed using a two-independent site binding model:

$$R_{obs}/R_{max} = R_1[(K_1P)/(1 + K_1P)] + R_2[(K_2P)/(1 + K_2P)] \quad (1)$$

where R_{obs} is the observed relative fluorescence increase, R_{max} is the maximum fluorescence increase observed at saturation, R_1 and R_2 are the maximum relative fluorescence increases corresponding to one and two C10 peptides bound, respectively, P is the peptide concentration, and K_1 and K_2 are macroscopic association constants for the binding of peptide to each site. Analysis of binding of C10 peptide to AtOASS at a high salt concentration (>0.5 M NaCl) used a single-site binding model to obtain the equilibrium binding constant, K_{eq}:

$$R_{obs}/R_{max} = (K_{eq}P)/(1 + K_{eq}P) \quad (2)$$

where R_{obs} is the observed relative fluorescence increase, R_{max} is the maximum fluorescence increase observed at saturation, and P is the peptide concentration. Fitting of data to either equation used Sigmaplot (Systat Software, Inc.) with the best-fit parameters selected on the basis of the lowest χ^2 values.

Calorimetric Measurements. Isothermal titration calorimetry (ITC) experiments were performed using a VP-ITC calorimeter (Microcal, Inc.). AtOASS and the C10 peptide were dialyzed overnight at 25 °C in 50 mM Hepes buffer (pH 7) and 50 mM NaCl at a 1:500 volume ratio, unless otherwise indicated. Similar specific activities were observed before and after dialysis. All samples and buffer solutions were degassed at room temperature prior to use. Briefly, injections of 10−12 μL of either C10 peptide or AtOASS were added using a computer-controlled 250 μL microsyringe at an interval of 5−6 min into the sample solution containing either AtOASS or C10 peptide. Control experiments using buffer determined the heat of dilution for each injection. Data obtained from the titration of C10 peptide with AtOASS were analyzed using either a two-independent site binding model (eq 3) or a sequential two-site binding model (eq 4):

$$Q_i^{tot} = V_0E_{tot}\{[(K_1P)/(1 + K_1P)]\Delta H_1\} + [(K_2P)/(1 + K_2P)]\Delta H_2 \quad (3)$$

$$Q_i^{tot} = V_0E_{tot}\{[\Delta H_1K_1P + (\Delta H_1 + \Delta H_2)K_1K_2P^2]/(1 + K_1P + K_1K_2P^2)\} \quad (4)$$

where Q_i^{tot} is total heat after the ith injection, V_0 is the volume of the calorimetric cell, K_1 and K_2 are the observed equilibrium constants for each site, and ΔH_1 and ΔH_2 are the corresponding enthalpy changes. For the forward titration experiment, P and E_{tot} are the free concentration of C10

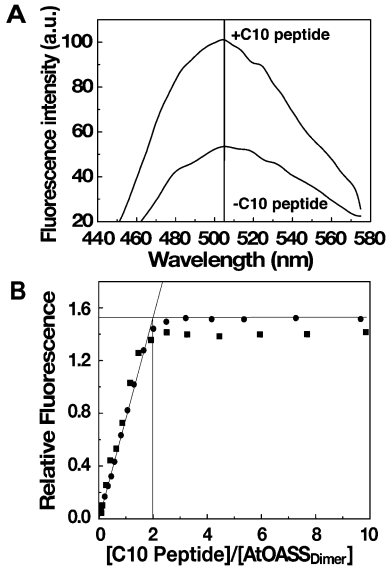

FIGURE 2: Fluorescence titration of AtOASS with C10 peptide. (A) Comparison of the fluorescence emission spectra of AtOASS (1 μM) in the absence and presence of C10 peptide (4 μM) in 50 mM Hepes (pH 7.0) with 20 mM NaCl. The excitation wavelength was 412 nm. (B) Fluorescence titration of 1 (●) and 2 μM (■) AtOASS in 50 mM Hepes (pH 7.0) with 20 mM NaCl. The break point at which the fluorescence signal does not increase is ~2.0, indicating that 2 mol of C10 peptide binds per AtOASS dimer.

peptide and the total concentration of AtOASS, respectively. In the reverse titration experiment, these are reversed. Estimates of K_{obs} and ΔH were obtained by fitting the experimental data to either model using software provided by the manufacturer of the instrument (Microcal, Inc.). The best-fit parameters were selected on the basis of the lowest χ^2 values. Values for the change in free energy (ΔG) were calculated using the relation $\Delta G = -RT \ln(K_{obs})$, where R is the gas constant (1.9872 cal K^{-1} mol^{-1}) and T the absolute temperature. Changes in entropy (ΔS) were calculated using the relation $\Delta G = \Delta H - T\Delta S$.

RESULTS

Estimation of C10 Peptide Binding Stoichiometry and Affinity by Fluorescence Spectroscopy. The active site PLP molecule shows a strong absorption band at 412 nm indicative of the presence of a Schiff base formed with Lys46 (*1*). Excitation of PLP at 412 nm generates an emission spectrum with maxima around 505 nm (Figure 2A). Titration of AtOASS with the C10 peptide shows increased PLP fluorescence (Figure 2B). Thus, monitoring the fluorescence emission changes after addition of the C10 peptide to AtOASS provides a signal for complex formation. The results of titrations performed at two different protein concentrations are shown in Figure 2B. In each titration, the relative fluorescence increases linearly with addition of C10 peptide, reaching a plateau upon saturation of AtOASS binding sites, indicating a maximum binding of two C10 peptides per AtOASS dimer. Titration results were independent of protein concentration and suggest tight binding of the C10 peptide such that only a lower limit for binding affinity could be estimated. Fitting of the binding isotherm to a two-site binding model (eq 1) yields similar values for K_1 and K_2 for each binding site (Table 1).

Determination of C10 Peptide Binding Energetics and Stoichiometry by ITC. To validate the fluorescence binding experiment and to further examine the energetics governing the interaction between the C10 peptide and AtOASS, we used ITC. The binding stoichiometry and energetics of complex formation using forward and reverse titrations were determined under the same conditions used in the fluorescence experiments. All titrations were corrected for addition of buffer alone to the sample chamber. Addition of C10 peptide to a solution of AtOASS shows that 1 mol of AtOASS dimer binds 2 mol of C10 peptide (Figure 3A). The binding isotherm fits to a two-independent site model (eq 3) with similar values for each binding site (Table 1). Data for the reverse titration experiment, i.e., injection of AtOASS into a solution of C10 peptide, are shown in Figure 3B. Fitting of the reverse titration binding isotherm to a two-site model yields similar values for each binding site (Table 1). ITC data in Figure 3 are plotted as kilocalories per mole of injectant. A summary of the energetics of complex formation from both the forward and reverse titrations is presented in Table 1.

Temperature Dependence of C10 Peptide Binding. To obtain insight into the forces driving the interaction between AtOASS and the C10 peptide, complex formation was examined as a function of temperature (10−35 °C). The binding isotherms obtained at different temperatures (Figure 4A) were all sigmoidal except at 35 °C. A comparison of data obtained at 25 and 35 °C is shown in Figure 4B. At temperatures up to 30 °C, the experimental data fit to a two-independent site model with each site having similar parameter values. Thus, C10 peptide binding at lower temperatures is not accompanied by any apparent cooperativity (Table 2). Overall, as the temperature increases, the binding enthalpies are negative with their magnitude increasing (Figure 4A and Table 2). The enthalpy for binding under the salt conditions that were used (50 mM NaCl) at 25 °C is similar to that observed with 20 mM NaCl at the same temperature (Table 1).

The binding isotherm at 35 °C exhibits more asymmetry than at other temperatures (Figure 4B). The transition from a sigmoidal shape to a nonsigmoidal likely occurs between 30 and 35 °C, but the effect is pronounced at 35 °C. The 35 °C experimental data were fit to both two independent site and sequential site binding models (Figure 4C). As shown, the fit to a sequential site binding model represents the data very well and yields two distinct macroscopic association constants (K_1 and K_2) for the binding of each C10 peptide to AtOASS (Table 2). Binding of the C10 peptide at 35 °C is 4-fold tighter than binding at 30 °C. Binding of the first C10 peptide is 8-fold tighter than binding of the second peptide. This suggests that at 35 °C, binding of the C10 peptide at one site decreases the intrinsic affinity at the second site and indicates negative cooperativity in the AtOASS homodimer. Therefore, temperature plays a role in dictating the nature of interaction between SAT and OASS.

Temperature Dependence of the Thermodynamic Parameters and Heat Capacity Change for the Interaction between AtOASS and the C10 Peptide. ITC provides a direct measurement of the enthalpy and analysis of free energy and entropy changes. Table 2 summarizes the measured enthalpy, free energy, and entropy changes for the interaction between AtOASS and the C10 peptide. These data are plotted as a

Table 1: Comparison of Binding of the C10 Peptide to AtOASS by Fluorescence Titration and ITC[a]

	stoichiometry	$K_{1,2}$ (M^{-1})	K_d (nM)	$\Delta G_{1,2}$ (kcal/mol)	$\Delta H_{1,2}$ (kcal/mol of C10 peptide)
fluorescence	2.0 ± 0.1	$(1.0 \pm 0.1) \times 10^8$	10.0 ± 1.0	–	–
ITC (forward)	1.9 ± 0.1	$(6.8 \pm 0.9) \times 10^7$	14.7 ± 1.9	-10.7 ± 0.1	-12.7 ± 0.1
ITC (reverse)	1.9 ± 0.1	$(7.5 \pm 0.8) \times 10^7$	13.3 ± 1.4	-10.7 ± 0.1	-11.0 ± 0.4

[a] Titrations were performed in 50 mM Hepes buffer (pH 7) with 20 mM NaCl at 22 °C, as described in Experimental Procedures. All data were fit to a two-independent site binding model that yielded similar values of K_{eq}, ΔG, and ΔH for each site, which are expressed as $K_{1,2}$, $\Delta G_{1,2}$, and $\Delta H_{1,2}$, respectively.

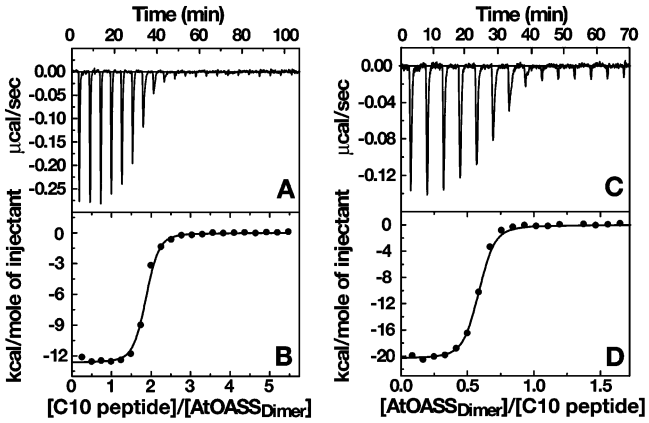

FIGURE 3: ITC analysis of the interaction between AtOASS and the C10 peptide. (A) Titration of AtOASS (2 μM) with C10 peptide (62.6 μM) at 25 °C in 50 mM Hepes (pH 7) with 20 mM NaCl. Data are plotted as the heat signal (microcalories per second) vs time (minutes). (B) Integrated heat responses per injection from panel A plotted as normalized heat per mole of injectant. The solid line represents the best fit of the data to a two-independent site binding model (eq 3). (C) Reverse titration of C10 peptide (2 μM) with AtOASS (21.0 μM) at 25 °C in 50 mM Hepes (pH 7) with 20 mM NaCl. Data are plotted as the heat signal (microcalories per second) vs time (minutes). (D) Integrated heat responses per injection from panel C plotted as normalized heat per mole of injectant. The solid line represents the best fit of the data to a two-independent site binding model (eq 3).

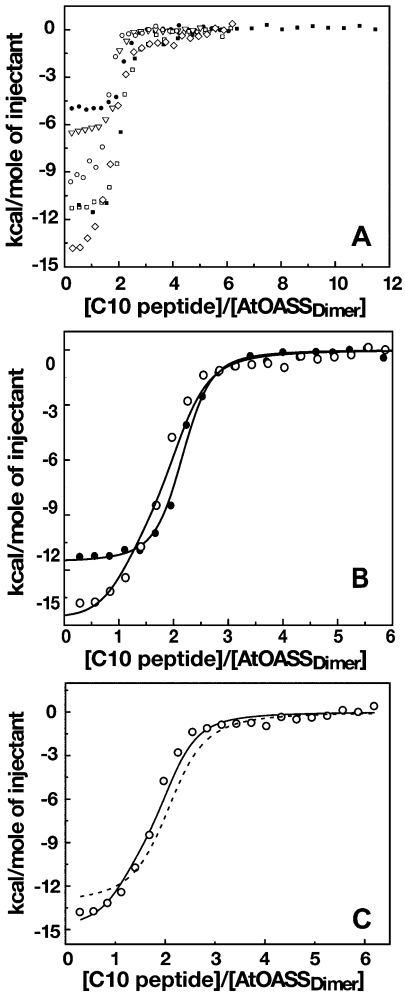

FIGURE 4: Temperature dependence of binding of C10 peptide to AtOASS. (A) ITC binding isotherms at different temperatures are shown, as follows: 10 (●), 15 (▽), 20 (○), 25 (□), 30 (■), and 35 °C (◇). Titrations were performed in 50 mM Hepes buffer (pH 7) with 50 mM NaCl. (B) Comparison of titrations of AtOASS with C10 peptide at 25 (●) and 35 °C (○). Data are plotted as normalized heat released per mole of C10 peptide vs the molar ratio of peptide to AtOASS dimer. At 25 °C, AtOASS and C10 peptide concentrations are 0.68 and 21.8 μM, respectively. The AtOASS and C10 peptide concentrations are 0.65 and 23.0 μM, respectively, at 35 °C. The binding isotherm at 25 °C was fit using a two-independent site binding model, and the 35 °C data were fit to a sequential binding model. (C) Comparison of data fitting to the 35 °C data. The solid line is the fit of the data to a sequential binding model. The dashed line shows the fit of the same data to a two-independent site binding model.

function of temperature in Figure 5A. The negative enthalpy of binding at all the temperatures that were examined (Table 2) indicates favorable exothermic binding interaction between the C10 peptide and AtOASS. At lower temperatures (10 and 15 °C), the entropic contribution is more favorable and decreases with an increase in temperature. This suggests that at lower temperatures, the association is driven by both enthalpy and entropy; however, the enthalpy of binding becomes the dominant force at higher temperatures.

The observed enthalpy depends linearly on the experimental temperature in the range of 10−35 °C. To determine the change in heat capacity (ΔC_p), the first derivative of temperature dependence of enthalpy change, the data were plotted as ΔH versus temperature (Figure 5B) to yield a ΔC_p of -0.401 ± 0.025 kcal mol^{-1} K^{-1}. The negative value of ΔC_p indicates that the binding is specific and accompanied by burial of nonpolar surface area (*22*, *23*). In addition, the negative ΔC_p causes the net thermodynamic force of complex formation to shift from a predominantly entropic contribution to an enthalpy-driven one as the temperature increases. The local interpolation of thermodynamic parameters (Figure 5A) indicates that at ~22 °C (T_S), the entropic contribution to the binding process is zero. This is the temperature at which the binding process becomes completely driven by enthalpy. In contrast, a linear fit of the binding enthalpy indicates that at −3.0 °C (T_H), the net enthalpic contribution is ~0 kcal/mol, with the binding process driven completely by entropy. Thus, between −3.0 and 22 °C, both enthalpy and entropy contribute favorably to the Gibbs energy of complex formation.

Table 2: ITC Analysis of the Temperature Dependence of Binding of the C10 Peptide to AtOASS[a]

temp (°C)	stoichiometry	$K_{1,2}$ (M^{-1})	K_d (nM)	$\Delta G_{1,2}$ (kcal/mol)	$\Delta H_{1,2}$ (kcal/mol)	$-T\Delta S_{1,2}$ (kcal/mol)
10[b]	2.0 ± 0.1	(1.7 ± 0.2) × 10^8	5.9 ± 0.7	−10.7 ± 0.1	−5.0 ± 0.1	5.3
15[b]	1.9 ± 0.1	(2.9 ± 0.3) × 10^8	3.5 ± 0.4	−11.1 ± 0.1	−6.3 ± 0.1	4.5
20[b]	2.0 ± 0.1	(9.1 ± 1.3) × 10^7	11.0 ± 1.6	−10.7 ± 0.1	−7.8 ± 0.1	2.9
25[b]	2.1 ± 0.1	(6.0 ± 0.5) × 10^7	16.7 ± 1.4	−10.6 ± 0.1	−11.6 ± 0.1	−1.4
30[b]	1.9 ± 0.1	(3.3 ± 0.3) × 10^7	30.3 ± 2.8	−10.4 ± 0.1	−13.0 ± 0.4	−3.0
35[c]	2.0 ± 0.1	(1.4 ± 0.3) × 10^8	7.1 ± 1.5	−11.5 ± 0.7	−14.6 ± 0.7	−3.1
		((1.7 ± 0.4) × 10^7)	(58.8 ± 13.8)	(−10.2 ± 0.2)	(−10.2 ± 0.8)	(0.0)

[a] Titrations were performed 50 mM Hepes buffer (pH 7) with 50 mM NaCl, as described in Experimental Procedures. [b] Data were fit to a two-independent site binding model that yielded similar values of K_{eq}, ΔG, ΔH, and $-T\Delta S$ for each site, which are expressed as $K_{1,2}$, $\Delta G_{1,2}$, $\Delta H_{1,2}$, and $-T\Delta S_{1,2}$, respectively. [c] Data were fit to a two-sequential site binding model that yielded different values of K_{eq}, ΔG, ΔH, and $-T\Delta S$ for each site. Values for binding of the second peptide are shown in parentheses.

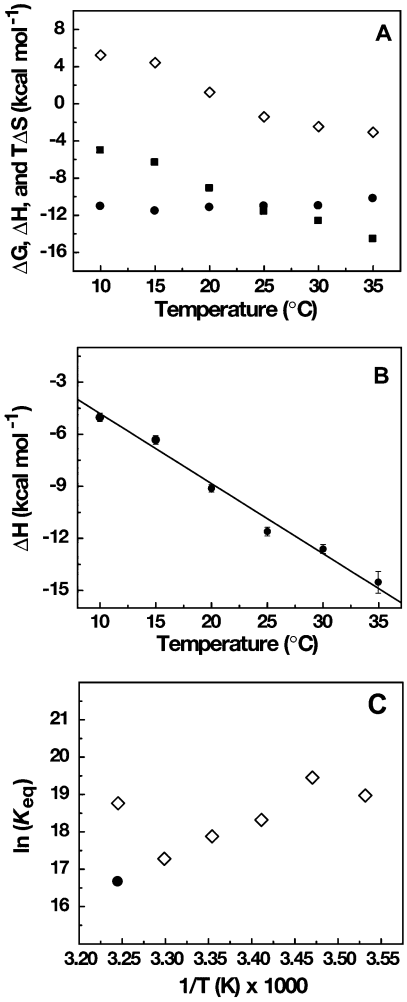

FIGURE 5: Temperature dependence of thermodynamic parameters for binding of C10 peptide to AtOASS. (A) Temperature dependence of ΔH (●), ΔG (■), and $-T\Delta S$ (◇) for the interaction. Error bars represent the standard deviation of the nonlinear least-squares fit to the raw data points. (B) Determination of heat capacity change (ΔC_p). (C) van't Hoff plot of K_{eq} vs temperature for formation of the AtOASS·C10 peptide complex. The K_{eq} values for binding of the first (◇) and second (●) C10 peptide at 35 °C are both shown.

Previous studies indicate that the linkage of interactions or conformational changes during binding may affect the van't Hoff plot (*24*, *25*). The temperature dependence of the equilibrium intrinsic binding constants for formation of the AtOASS·C10 peptide complex shows a nonlinear van't Hoff plot (Figure 5C), suggesting that the interaction could be linked with other processes, including potential conformational changes. The intrinsic binding constants increase with a decrease in temperature, reaching the highest value at 15 °C and then decreasing with temperature. Interestingly, the binding constant for the binding of the first peptide increases at 35 °C compared to a decrease in the same for binding of the second peptide. The general dependence of the binding constants at 10−30 °C follows a similar trend, but at 35 °C, the trend is reversed. This divergent behavior at 35 °C increases the magnitude of the difference between their values, which is reflected in the apparent negative cooperativity.

Ionic Dependence of C10 Peptide Binding. The structure of the AtOASS·C10 peptide complex suggests that hydrophobic interactions and hydrogen bonds between the protein and peptide are involved in binding (*18*). To obtain information about the electrostatic properties of the interaction between AtOASS and the C-terminus of AtSAT, we tested the effect of NaCl on C10 peptide binding. The fluorescence of PLP was used to monitor C10 peptide binding (Figure 2A). To confirm that changes in salt concentration did not alter oligomerization of AtOASS, gel filtration chromatography showed that the protein was a stable homodimer at the salt concentrations that were used (not shown). The results of titrations performed as a function of NaCl concentration are shown in Figure 6A. Equilibrium binding constants were determined for the interaction of the C10 peptide with AtOASS in the presence of up to 1.3 M NaCl (Table 3). Comparison of the binding affinity for the C10 peptide binding over the NaCl concentration range that was used shows two distinct phases of behavior (Figure 6B). Initially, the K_{eq} values decrease as the salt concentration increases. Then, at higher NaCl concentrations, the affinity for the C10 peptide becomes independent of salt concentration. In addition, the stoichiometry switches from two-site occupancy at lower salt concentrations to single-site binding at >0.5 M NaCl. The effect of salt on C10 peptide binding is also observed in the R_{max} values (Figure 6C), which suggest that high ion concentrations prevent binding of the second C10 peptide. A linear fit of the data yields a slope of 0.9 ± 0.1, indicating that binding of the C10 peptide to AtOASS is accompanied by the release of one anion or cation.

DISCUSSION

Here we present a series of binding experiments that for the first time analyze the detailed thermodynamic properties of formation of a complex between AtOASS and the C-terminal ligand of AtSAT. Assembly of the cysteine synthase complex in plants and bacteria has been demonstrated multiple times (*9*−*16*), but a systematic examination

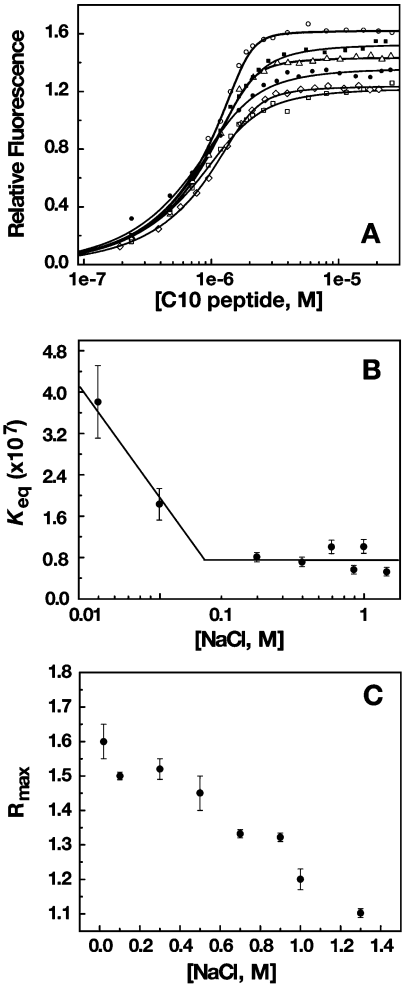

FIGURE 6: Salt dependence of formation of the AtOASS·C10 peptide complex. (A) Fluorescence titration of AtOASS with C10 peptide as a function of NaCl concentration. The solid lines are nonlinear least-squares fits of the titration curves using either eq 1 or 2. (B) Effect of salt concentration on K_{eq} for the binding of a single C10 peptide to AtOASS. (C) Relative fluorescence increase (R_{max}) as a function of NaCl concentration.

Table 3: Fluorescence Titration Analysis of the Salt Dependence of Interaction between AtOASS and the C10 Peptide[a]

[NaCl] (M)	stoichiometry	K_{eq} (M^{-1})	K_d (nM)	R_{max}
0.05[b]	2	$(4.5 \pm 0.7) \times 10^7$	22.2 ± 3.4	1.60 ± 0.05
0.1[b]	2	$(1.8 \pm 0.3) \times 10^7$	55.6 ± 9.3	1.52 ± 0.01
0.3[b]	2	$(8.0 \pm 0.3) \times 10^6$	125 ± 5	1.52 ± 0.03
0.5[b]	2	$(7.0 \pm 0.6) \times 10^6$	143 ± 12	1.45 ± 0.05
0.7[c]	1	$(1.0 \pm 0.1) \times 10^7$	100 ± 10	1.33 ± 0.01
0.9[c]	1	$(6.0 \pm 0.8) \times 10^6$	167 ± 22	1.32 ± 0.01
1.0[c]	1	$(1.0 \pm 0.1) \times 10^7$	100 ± 11	1.20 ± 0.03
1.3[c]	1	$(5.0 \pm 0.9) \times 10^6$	200 ± 36	1.10 ± 0.02

[a] Titrations were performed in 50 mM Hepes buffer (pH 7) with 20 mM NaCl at 22 °C, as described in Experimental Procedures. [b] Data were fit to a two-independent site binding model that yielded similar values of K_{eq} for each site. [c] Data were fit to a single-site binding model.

of the energetics of the association of OASS and SAT has not been undertaken. Although protein−protein interactions differ from protein−peptide interactions in the size of one interaction partner, variations in the well-defined structures of both molecules, and changes in the entropy of interaction due to mobility and solvent organization between protein and a representative peptide, the use of simplified systems allows the dissection of the molecular mechanisms of complex formation (*26*).

The interaction between AtOASS and AtSAT can be effectively studied using the C10 peptide because the 10−20 C-terminal amino acids of SAT are unstructured in solution (*27*−*29*) and deletion of the 10 C-terminal residues or mutations at key positions abrogates interaction of SAT with OASS (*10*−*12*, *16*, *18*). Moreover, in the crystal structures of OASS in complex with the C10 peptide (*17*, *18*), the ligand lacks secondary structure and analysis of the C10 peptides structure by circular dichroism shows no structural changes occur under the range of experimental conditions used here (not shown). The binding constants for formation of the AtOASS·C10 peptide complex (Tables 1 and 2) are similar to those reported for association of full-length AtSAT and AtOASS (*13*). Using surface plasmon resonance (or BIAcore analysis), Berkowitz et al. (*13*) showed that interaction between the two plant proteins is tight with a K_d of 25 nM. The fluorescence and ITC binding studies presented here yield similar binding affinities (K_d = 10−40 nM) depending upon solution conditions. Thus, the C-terminus of AtSAT contributes significantly to the total free energy of interaction with AtOASS. In contrast, formation of the bacterial cysteine synthase complex may involve additional protein−protein interactions, since the affinity of the bacterial OASS for the full-length bacterial SAT is tighter than binding of the corresponding C10 peptide alone (*10*, *11*, *15*). This difference may reflect structural differences in the assembly of the plant and bacterial cysteine synthase complexes.

It is likely that thermodynamic parameters, i.e., salt dependence and the temperature dependence of ΔH, for the interaction between full-length SAT and OASS will be quantitatively different from those for the OASS−C10 peptide interaction. For example, the net entropy change upon binding may be less favorable for the C10 peptide interaction than for binding of full-length SAT. Moreover, the temperature dependence of binding enthalpy for the interaction between full-length SAT and OASS may involve additional contributions from other coupled equilibria such as conformation changes or proton−ion exhanges (*26*).

In the plant OASS, reports of positive cooperativity during substrate (*O*-acetylserine) binding suggest that structural changes during the catalytic cycle may mediate allosteric communication between the active sites in the homodimer (*13*, *30*, *31*). To account for potential cooperativity upon C10 peptide binding, the fluorescence and ITC binding studies were analyzed using a two-independent site binding model. Our results suggest that the two binding sites of AtOASS are symmetric in nature and that binding of C10 peptide at one site is independent of binding at the second site over broad temperature (10−30 °C) and salt (0.02−0.5 M NaCl) ranges. These results are consistent with the structures of AtOASS alone and in complex with the C10 peptide that show no global structural differences are induced upon peptide binding (*15*, *18*). Interestingly, negative cooperativity for binding of the C10 peptide to AtOASS occurs at a higher temperature (35 °C). At lower temperatures, hydrogen bond and electrostatic interactions are strong with hydrophobic interactions weaker in protein structures, whereas the reverse is true at higher temperatures (*32*). Temperature-related

changes in protein structure could affect cooperative behavior in both catalysis and ligand binding (*33*), but the details of these differences are unclear.

Thermodynamic analysis of the interaction between AtOASS and the C10 peptide indicates that the free energy of binding varies only slightly over the temperature range that was examined with the entropic and enthalpic contributions to the association process varying with temperature in a compensatory fashion (Table 2 and Figure 5). At lower temperatures, both enthalpy and entropy contribute to binding interactions, but with an increase in temperature, the enthalpic contribution increases and the entropic contribution decreases. The release of nonspecifically bound water molecules from AtOASS upon C10 peptide binding at lower temperatures would increase the net entropy of the system, thereby contributing to the free energy of interaction (*34*). It should be noted that the structure of the AtOASS·C10 peptide complex exhibited a number of water-mediated interactions (*18*), indicating that specifically bound water molecules are not released and likely contribute to binding affinity at lower temperatures. At higher temperatures, there is sufficient energy in the system to disrupt weakly bound water molecules and decrease the favorable entropy component of peptide binding. The differential solvation state of AtOASS is also reflected in the nonlinear temperature dependence of K_{eq}, as observed in the van't Hoff plot (Table 2 and Figure 5C). Although a preexisting conformational equilibrium of an unbound form of an interaction partner may influence the temperature dependence of binding (*35*), this is not the case here because circular dichroism spectroscopy showed no structural changes in either AtOASS or C10 peptide over the temperature range used in this study (data not shown).

Changes in protein dynamics are often reflected in the thermodynamic profiles of protein−protein interactions (*36*). Analysis of AtOASS·C10 peptide complex formation shows that the values of ΔH are linearly dependent on temperature and that the heat capacity change is modest and negative ($\Delta C_p = -401$ cal mol^{-1} K^{-1}). The magnitude of the ΔC_p value implies that interaction between the two molecules is not accompanied by a major conformational change, as suggested by circular dichroism spectroscopy, although the interaction does not appear to be a perfect rigid body association as indicated by a low T_s value (22 °C) (*22*). Calculation of the estimated change in heat capacity (ΔC_p^{calc}) from the difference in accessible surface area between the free and peptide-bound forms of AtOASS (*14*, *18*) was carried out as follows (*37*):

$$\Delta C_p^{calc} = 0.45(\Delta\text{available nonpolar surface area}) - 0.26\,(\Delta\text{available polar surface area}) \quad (5)$$

The ΔC_p^{calc} is −273 cal mol^{-1} K^{-1}, which is smaller than the experimentally determined value. The difference between the experimental and calculated values suggests that binding of C10 peptide to AtOASS may cause additional localized conformational changes in solution that are not observed in the crystal structures of the enzyme (*15*, *18*).

The change in heat capacity indicates burial of nonpolar surface area during binding of the C10 peptide by AtOASS, but structural studies show that hydrogen bonds and hydrophobic interactions are involved in binding of the ligand (*18*). The contribution of electrostatics to binding was examined by determining the ionic dependence of association (Figure 6 and Table 3). Association of the C10 peptide with AtOASS is sensitive to salt concentration with binding affinity decreasing 6-fold from 0.05 to 0.5 M NaCl, which indicates an only modest electrostatic contribution to binding. Typical electrostatically driven interactions display greater changes in equilibrium constants over a similar range of salt concentrations. For example, the affinity of binding of phosphopeptide to Src homology 2 (SH2) domains undergoes 100−1000-fold changes over the same salt concentrations (*38*). The electrostatic contribution to C10 peptide binding may derive from hydrogen bonds formed between the C-terminal carboxylate group of the peptide and amino acid side chains in the AtOASS active site (*18*). Nonetheless, this result indicates that the binding energy for formation of the AtOASS·C10 peptide complex is primarily derived from nonelectrostatic interactions.

At NaCl concentrations above 0.5 M, interaction between the C10 peptide and AtOASS becomes independent of ionic environment. Likewise, the stoichiometry of peptide binding changes. Binding of anions at an allosteric site on the OASS from *Salmonella typhimurium* induces a conformational change that prevents substrate binding and catalysis (*39*, *40*). Although no evidence for an allosteric site has been reported for the plant OASS, high salt concentrations may cause structural changes that affect interaction with the C-terminus of SAT; however, the changes in binding associated with high salt concentrations (>0.5 M NaCl) are likely not biologically relevant, since NaCl concentrations above 0.1 M cause severe and toxic salt stress in plants (*41*, *42*). Although NaCl inhibits the activity of OASS from *S. typhimurium* ($K_i = 20$ mM) (*40*), AtOASS activity is affected by only nonphysiological levels of NaCl ($IC_{50} > 1$ M NaCl). Thus, the effects observed at lower salt concentrations (0−0.5 M) likely do not reflect inhibition of the enzyme.

Physiologically, temperature changes affect sulfur assimilation and cysteine biosynthesis in plants (*43*−*46*). Elevated temperatures (>35 °C) reduce the demand for cysteine (*43*), whereas increased sulfur utilization and cysteine production provide needed metabolites for glutathione synthesis in response to low-temperature chilling (*44*−*46*). Since formation of the plant cysteine synthase complex is associated with increased SAT activity (*6*, *8*), the temperature-dependent interaction of OASS and SAT may contribute to modulating cysteine synthesis in plants. As shown here, the affinity of the interaction between AtOASS and the C10 peptide is greater at low temperatures with decreased affinity and negative cooperativity observed at higher temperatures. The thermodynamics of the OASS−SAT interaction parallels the demands placed on cysteine synthesis in response to temperature.

ACKNOWLEDGMENT

We thank Dr. Xuemin (Sam) Wang for generous access to the ITC instrument in his lab and Dr. Carl Frieden for use of his lab's CD spectrometer.

REFERENCES

1. Rabeh, W. M., and Cook, P. F. (2004) Structure and mechanism of O-acetylserine sulfhydrylase, *J. Biol. Chem. 279*, 26803−26806.

2. Wirtz, M., and Droux, M. (2005) Synthesis of the sulfur amino acids: Cysteine and methionine, *Photosynth. Res. 86*, 345−346.
3. Kopriva, S. (2006) Regulation of sulfate assimilation in *Arabidopsis* and beyond, *Ann. Bot. 97*, 479−495.
4. Kredich, N. M., Becker, M. A., and Tomkins, G. M. (1969) Purification and characterization of cysteine synthetase, a bifunctional protein complex, from *Salmonella typhimurium*, *J. Biol. Chem. 244*, 2428−2439.
5. Cook, P. F., and Wedding, R. T. (1977) Initial kinetic characterization of the multienzyme complex, cysteine synthetase, *Arch. Biochem. Biophys. 178*, 293−302.
6. Droux, M., Ruffet, M. L., Dounce, R., and Job, B. (1998) Interactions between serine acetyltransferase and O-acetylserine-(thiol)lyase in higher plants: Structural and kinetic properties of the free and bound enzymes, *Eur. J. Biochem. 255*, 235−245.
7. Hell, R., and Hillebrand, H. (2001) Plant concepts for mineral acquisition and allocation, *Curr. Opin. Biotechnol. 12*, 161−168.
8. Saito, K., Yokoyama, H., Noji, M., and Murakoshi, I. (1995) Molecular cloning and characterization of a plant serine acetyltransferase playing a regulatory role in cysteine biosynthesis from watermelon, *J. Biol. Chem. 270*, 16321−16326.
9. Bogdanova, N., and Hell, R. (1997) Cysteine synthesis in plants: Protein-protein interactions of serine acetyltransferase from *Arabidopsis thaliana*, *Plant J. 11*, 251−262.
10. Mino, K., Yamanoue, T., Sakiyama, T., Eisaki, N., Matsuyama, A., and Nakanishi, K. (1999) Purification and characterization of serine acetyltransferase from *Escherichia coli* partially truncated at the C-terminal region, *Biosci., Biotechnol., Biochem. 63*, 168−179.
11. Mino, K., Hiraoka, K., Imamura, K., Sakiyama, T., Eisaki, N., Matsuyama, A., and Nakanishi, K. (2000) Characteristics of serine transacetylase from *Escherichia coli* deleting different lengths of amino acid residues from the C-terminus, *Biosci., Biotechnol., Biochem. 64*, 1874−1880.
12. Wirtz, M., Berkowitz, O., Droux, M., and Hell, R. (2001) The cysteine synthase complex in plants: Mitrochondrial serine acetyltransferase from *Arabidopsis thaliana* carries a bifunctional domain for catalysis and protein-protein interaction, *Eur. J. Biochem. 268*, 686−693.
13. Berkowitz, O., Wirtz, M., Wolf, A., Kuhlmann, J., and Hell, R. (2002) Use of biomolecular interaction analysis to elucidate the regulatory mechanism of the cysteine synthase complex from *Arabidopsis thaliana*, *J. Biol. Chem. 277*, 30629−30634.
14. Bonner, E. R., Cahoon, R. E., Knapke, S. M., and Jez, J. M. (2005) Molecular basis of cysteine biosynthesis in plants: Structural and functional analysis of O-acetylserine sulfhydrylase from *Arabidopsis thaliana*, *J. Biol. Chem. 280*, 38803−38813.
15. Campanini, B., Speroni, F., Salsi, E., Cook, P. F., Roderick, S. L., Huang, B., Bettati, S., and Mozzarelli, A. (2005) Interaction of serine acetyltransferase with O-acetylserine sulfhydrylase active site: Evidence from fluorescence spectroscopy, *Protein Sci. 14*, 2115−2124.
16. Zhao, C., Moriga, Y., Feng, B., Kumada, Y., Imanaka, H., Imamura, K., and Nakanishi, K. (2006) On the interaction site of serine acetyltransferase in the cysteine synthase complex from *Escherichia coli*, *Biochem. Biophys. Res. Commun. 341*, 911−916.
17. Huang, B., Vetting, M. W., and Roderick, S. L. (2005) The active site of O-acetylserine sulfhydrylase is the anchor point for bienzyme complex formation with serine acetyltransferase, *J. Bacteriol. 187*, 3201−3205.
18. Francois, J. A., Kumaran, S., and Jez, J. M. (2006) Structural basis for interaction of O-acetylserine sulfhydrylase and serine acetyltransferase in the plant cysteine synthase complex, *Plant Cell 18*, 3647−3655.
19. Kawashima, C. G., Berkowitz, O., Hell, R., Noji, M., and Saito, K. (2005) Characterization and expression of a serine acetyltransferase gene family involved in a key step of sulfur assimilation in *Arabidopsis*, *Plant Physiol. 137*, 220−230.
20. Gill, S. C., and von Hippel, P. H. (1989) Calculation of protein extinction coefficients from amino acid sequence data, *Anal. Biochem. 182*, 319−326.
21. Lohman, T. M. (1992) *Escherichia coli* DNA helicases: Mechanisms of DNA unwinding, *Mol. Microbiol. 6*, 5−14.
22. Spolar, R. S., and Record, M. T. (1994) Coupling of local folding to site-specific binding of proteins to DNA, *Science 263*, 777−784.
23. O'Brien, R., DeDecker, B., Fleming, K. G., Sigler, P. B., and Ladbury, J. E. (1998) The effects of salt on TATA-binding protein-DNA interactions from a hyperthermophili archaeon, *J. Mol. Biol. 279*, 117−123.
24. Horn, J. R., Brandts, J. F., and Murphy, K. P. (2002) van't Hoff and calorimetric enthalpies II: Effects of linked equilibria, *Biochemistry 41*, 7501−7507.
25. Kumaran, S., Grucza, R. A., and Waksman, G. (2003) The tandem Src homology 2 domain of the Syk kinase: A molecular device that adapts to interphosphotyrosine distances, *Proc. Natl. Acad. Sci. U.S.A. 100*, 14828−14833.
26. Stites, W. E. (1997) Protein-protein interactions: Interface structure, binding thermodynamics, and mutational analysis, *Chem. Rev. 97*, 1233−1250.
27. Olsen, L. R., Huang, B., Vetting, M. B, and Roderick, S. L. (2004) Structure of serine acetyltransferase in complexes with CoA and its cysteine feedback inhibitor, *Biochemistry 43*, 6013−6019.
28. Pye, V. E., Tingey, A. P., Robson, R. L., and Moody, P. C. E. (2004) The structure and mechanism of serine acetyltransferase from *Escherichia coli*, *J. Biol. Chem. 279*, 40729−40736.
29. Gorman, J., and Shapiro, L. (2004) Structure of serine acetyltransferase from *Haemophilus influenzae*, *Acta Crystallogr. D60*, 1600−1605.
30. Kuske, C. R., Ticknor, L. O., Guzman, E., Gurley, L. R., Valdez, J. G., Thompson, M. E., and Jackson, P. J. (1994) Purification and characterization of O-acetylserine sulfhydrylase isoenzymes from *Datura innoxia*, *J. Biol. Chem. 269*, 6223−6232.
31. Rolland, N., Ruffet, M. L., Job, D., Douce, R., and Droux, M. (1996) Spinach chloroplast O-acetylserine(thiol)-lyase exhibits two catalytically non-equivalent pyridoxal-5′-phosphate-containing active sites, *Eur. J. Biochem. 236*, 272−282.
32. Creighton, T. E. (1993) *Proteins: Structures and molecular properties*, 2nd ed., W. H. Freeman & Co., New York.
33. Giordano, A., Febbraio, F., Russo, C., Rossi, M., and Raia, C. A. (2005) Evidence for co-operativity in coenzyme binding to tetrameric *Sulfolobus solfataricus* alcohol dehydrogenase and its structural basis: Fluorescence, kinetic and structural studies of the wild-type enzyme and non-co-operative N249Y mutant, *Biochem. J. 388*, 657−667.
34. Ortiz-Salmeron, E., Yassin, Z., Clemente-Jimenez, M. J., Las Heras-Vazquez, F. J., Rodriguez-Vico, F., Baron, C., and Garcia-Fuentes, L. (2001) Thermodynamic analysis of the binding of glutathione to glutathione S-transferase over a range of temperatures, *Eur. J. Biochem. 268*, 4307−4314.
35. Ferrari, M. E., and Lohman, T. M. (1994) Apparent heat capacity change accompanying a nonspecific protein-DNA interaction. *Escherichia coli* SSB tetramer binding to oligodeoxyadenylates, *Biochemistry 33*, 12896−12910.
36. Wang, C., Pawley, N. H., and Nicholson, L. K. (2001) The role of backbone motions in ligand binding to the c-Src SH3 domain, *J. Mol. Biol. 313*, 873−887.
37. Fraczkiewicz, R., and Braun, W. (1998) Exact and efficient analytical calculation of the accessible surface areas and their gradients of macromolecules, *J. Comput. Chem. 19*, 319−333.
38. Grucza, R. A., Bradshaw, J. M., Mitaxov, V., and Waksman, G. (2000) Role of electrostatic interactions in SH2 domain recognition: Salt-dependence of tyrosyl-phosphorylated peptide binding to the tandem SH2 domain of the Syk kinase and the single SH2 domain of the Src kinase, *Biochemistry 39*, 10072−10081.
39. Burkhard, P., Tai, C. H., Jansonius, J. N., and Cook, P. F. (2000) Identification of an allosteric anion-binding site on O-acetylserine sulfhydrylase: Structure of the enzyme with chloride bound, *J. Mol. Biol. 303*, 279−286.
40. Tai, C. H., Burkhard, P., Gani, D., Jenn, T., Johnson, C., and Cook, P. F. (2001) Characterization of the allosteric anion-binding site of O-acetylserine sulfhydrylase, *Biochemistry 40*, 7446−7452.
41. Barroso, C., Romero, L. C., Cejudo, F. J., Vega, J. M., and Gotor, C. (1999) Salt-specific regulation of the cytosolic O-acetylserine-(thiol)lyase gene from *Arabidopsis thaliana* is dependent on abscisic acid, *Plant Mol. Biol. 40*, 729−736.
42. Ruiz, J. M., and Blumwald, E. (2002) Salinity-induced glutathione synthesis in *Brassica napus*, *Planta 214*, 965−969.

43. Nieto-Sotelo, J., and Ho, T. H. (1986) Effect of heat shock on the metabolism of glutathione in maize roots, *Plant Physiol. 82*, 1031−1035.
44. Kocsy, G., Szalai, G., Vagujfalvi, A., Stehli, L., Orosz, G., and Galiba, G. (2000) Genetic study of glutathione accumulation during cold hardening in wheat, *Planta 210*, 295−301.
45. Gomez, L. D., Vanacker, H., Buchner, P., Noctor, G., and Foyer, C. H. (2004) Intercellular distribution of glutathione synthesis in maize leaves and its response to short-term chilling, *Plant Physiol. 134*, 1662−1671.
46. Phartiyal, P., Kim, W. S., Cahoon, R. E., Jez, J. M., and Krishnan, H. B. (2006) Soybean ATP sulfurylase, a homodimeric enzyme involved in sulfur assimilation, is abundantly expressed in roots and induced by cold treatment, *Arch. Biochem. Biophys. 450*, 20−29.

BI7001168